***Final Draft***
**of the original manuscript:**

Knaapila, M.; Stepanyan, R.; Torkkeli, M.; Haramus, V.M.; Galbrecht, F.; Nehls, B.S.; Preis, E.; Scherf, U.; Monkman, A.P.:

**Control over phase behavior and solution structure of hairy-rod polyfluorene by means of side-chain length and branching**

In: Physical Review E (2008) APS

DOI: 10.1103/PhysRevE.77.051803

# Control over phase behavior and solution structure of hairy-rod polyfluorene by means of side chain length and branching

M. Knaapila,[1,*] R. Stepanyan,[2] M. Torkkeli,[3] V. M. Garamus,[4] F. Galbrecht,[5] B. S. Nehls,[5] U. Scherf,[5] and A. P. Monkman[6]

*[1] MAX-lab, Lund University, POB 118, SE-22100 Lund, Sweden, [2] Materials Science Centre, DSM Research, POB 18, NL-6160 MD Geleen, The Netherlands, [3] Department of Physical Sciences, POB 64, FI-00014 University of Helsinki, Finland, [4] GKSS Research Centre, Max-Planck-Strasse 1, D-21502 Geesthacht, Germany, [5] Bergische Universität Wuppertal, Gauß-Strasse 20, D-42097 Wuppertal, Germany, [6] Department of Physics, University of Durham, South Road, DH1 3LE Durham, UK*

36.20.-r Macromolecules and polymer molecules, 81.16.Dn Self-assembly, 82.35.Lr Physical properties of polymers, 64.60.Cn Order-disorder transformations; statistical mechanics of model systems

Suggested subject-matter section: Part 1: Statistical, soft-matter and biological physics: Polymers

*Author to whom correspondence should be addressed: Matti Knaapila, Tel: +46-46-22-24306, Fax: +46-46-22-24710, Electronic address: matti.knaapila@maxlab.lu.se

We present guidelines on how the solution structure of π-conjugated hairy-rod polymer can be designed by the side chain length and branching. First, the semi-quantitative mean field theory is formulated predicting a lyotropic phase with solvent coexistence and a metastable membrane phases in solution with increasing side chain length, $N$, the phase transition being at $N^*$. The membrane phase transforms into the isotropic phase of dissolved rodlike polymers at the temperature $T_{mem}^*(N) \sim N^{-1/2}$. $T_{mem}^*$ is proposed to decrease with increasing degree of side chain branching. Second, in experiment, poly(9,9-dialkylfluorene)s with $N = 6-10$ were employed in methylcyclohexane. The side chain branching was varied for $N = 8$ by using poly(9,9-dioctylfluorene)/(9,9-bis-(2-ethylhexyl)-fluorene) random copolymers with proportions of 9,9-dioctylfluorene to 2-ethylhexylfluorene monomers 100:0, 95:5, 90:10, 50:50, and 0:100. In qualitative accord with the theory, the lyotropic, membrane, and isotropic phases with the corresponding phase transitions are observed. $N^*$ is found for $\leq 6$ and $T_{mem}^*(N)$ decreases from 340 K to 280 K and scales as $\sim N^{-1/2}$ for $N \geq 8$. The membrane phase is found when the fraction of 9,9-dioctylfluorene monomers is at least 90%, $T_{mem}^*(N)$ decreasing with this fraction. In the membrane phase regime the system consists of dissolved polymers, loose sheets of two polymer layers and better packed sheets which are identified as so called beta phase. The connection of these fractions to the theoretical reasoning is discussed and their abundance measured for $T \leq T_{mem}^*$.

## I. INTRODUCTION

Understanding of macromolecular self-organization[1] is critical in the materials science of hairy-rod polymers[2]. An important class of self-assembling hairy rods are π-conjugated polymers[3] amongst which polyfluorenes (PFs)[4-7] ground myriad applications in solution processed polymer electronics[8]. The phase behavior of PFs has been extensively studied in the solid state but the literature of their solution assemblies remains not all-inclusive, specific exceptions including systems such as poly(9,9-dioctylfluorene) (PF8)[9-12], poly(9,9-bis(2-ethylhexyl)-fluorene-2,7-diyl) (PF2/6)[13, 14, 10], F2/6 oligomers[15], poly(9,9-dialkylfluorene-*co*-fluorenone) copolymers[16] and poly{2,7-(9,9-bis((*S*)-3,7-dimethyloctyl))fluorene}[17]. More systematic studies on the various aspects of solution assemblies would yet be advantageous not least because the solvent plays a chief role in morphology of the solvent processed thin films[18].

Theoretical phase behavior of hairy-rod solutions has been addressed by Ballauff[19] in a framework of a Flory lattice model. It has been shown that an isotropic solution of hairy-rods is stable only in a low concentration and high temperature regime. Upon increasing temperature the system phase separates into virtually pure solvent and lyotropic nematic with relatively high polymer concentration. The isotropic-nematic liquid transition temperature $T_{IN}$ * is a decreasing function of the side chain length, hence longer side chains postponing demixing. However, formation of any intermediate (possibly metastable) structure has been left out to this picture. We have hitherto shown that PFs provide a versatile tool to study the phase behavior of hairy-rods both theoretically and experimentally in the solid state and aligned films[7]. We propose that PFs can also constitute a valuable model system for the solution studies.

The solution behavior of PFs can be rationalized in terms of three experimental variables — the nature of solvent, the fraction of polymer, and the nature of side chain. The length of the polymer is another parameter becoming dominant for oligomers[15]. A major structural diversity arises from the quality of solvent, the first parameter. For example, PF8 forms sheetlike particles in 1 wt-% solution of a poor solvent methylcyclohexane (MCH) and a rodlike isotropic phase in a better solvent, toluene[10]. Alternatively, if the polymer fraction, the second parameter, is increased from 1 wt-% to 3-7 wt-% in toluene, stiff PF8 molecules turn to a large network-like structure[20].

In our previous work[10, 12] we studied the nature of side chain length, the third variable, using branched side chain PF2/6 and a series of linear side chain PFs — poly(9,9-dihexylfluorene) (PF6), poly(9,9-diheptylfluorene) (PF7), PF8, poly(9,9-dinonylfluorene) (PF9), and poly(9,9-didecylfluorene) (PF10) — in MCH. In MCH, PF6, PF7, PF8, and PF9 form sheet-like particles whereas PF2/6 and PF10 remain fully dissolved rodlike chains. In this work the experiments were performed at 20 $^{o}$C.

The photophysics of so called $\beta$ phase is another motivation for our phase behavioral investigations. The $\beta$ phase[9] is well-known for solid state PF8 that is polymorphic with a range of crystalline[21] and non-crystalline[22] phases. These phases originate from classes of conformational isomers (denoted as $C_{\alpha}$, $C_{\beta}$, ...), defined by the torsional angle between the repeat units[23, 24]. The $\beta$ phase is a solid state manifestation of the single isomer $C_{\beta}$ with torsional angle of 160-165$^{o}$. It is extraordinary amongst π-conjugated polymers with very narrow linewidths in its optical spectra[25] showing even potency in lasing[26]. As MCH mixtures of PF7, PF8, and PF9 contain large amount of this nearly

planar conformational isomer[12] the question remains whether its fraction could be controlled by nanoscale solution assemblies or whether the opposite is true.

The objectives of the present paper are as follows. Firstly, we aim at connecting the formation of 2-dimensional structures (or membranes) to the experimental framework of PFs as a function of side chain length $(N)$. Instead of focusing on room temperature, we probe full accessible temperature range. Secondly, we keep $N$ constant and vary the degree of side chain branching by means of copolymerization. We find that the lyotropic phase and the metastable (and potentially stable) membrane phase exist in solution with increasing $N$. The phase transition is observed at $N^* \sim 6$. The membrane phase turns to the isotropic phase of dissolved rodlike polymers at $T_{mem}^*(N = 7-10)$, this value sharply decreasing for $N \geq 8$. The side chain branching is also found to decrease $T^*(N = 8)$ and the membrane phase found when the fraction of linear chain monomers is at least 90%. The details of the polymer demixing and loose and better packed beta sheets are moreover given. These results form the principle on how the solution structure of hairy-rod polyfluorene can be controlled by the side chain length and side chain branching.

## II. THEORY

### A. Free energies

An idea of hairy-rod solution and a solution of 2-dimensional hairy-rod sheets (or membranes) is plotted in Fig. 1. Based on this scheme we estimate the scaling behavior of the transition temperature as a function of the side chain length as follows. First, the free energy of the isotropic solution phase reads as

$$F^{(sol)} = F_{brush}^{(sol)} + F_{RS}^{(sol)} + F_{RA}^{(sol)} + F_{tr}^{(sol)}, \quad (1)$$

where the brush term $F_{brush}^{(sol)}$ includes the excluded volume interaction between the alkyl chains in a good solvent and their stretch (which has been calculated e.g. in Ref. [27]). Per side chain this reads as

$$F_1^{(sol)} = k_B T \left( \frac{\nu N}{a^2 b} \right)^{1/2}, \quad (2)$$

where $\nu$ is the excluded volume of a side chain monomer in a good solvent, $N$ and $a$ the number of monomers per side chain and its statistical segment length, respectively. Here $b$ is the grafting distance along the backbone. The next two terms $F_{RS}^{(sol)}$ and $F_{RA}^{(sol)}$ represent the interaction of the backbone rod ("R") with solvent ("S") molecules and alkyl chains ("A"), respectively. Finally, the last term incorporates the translational free-energy of the hairy-rod molecules.

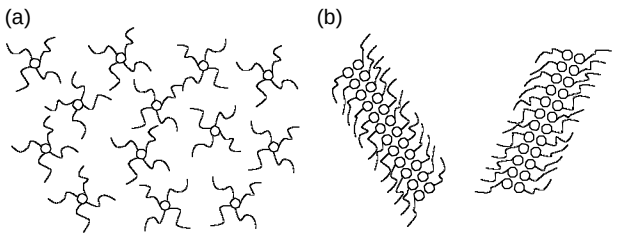


FIG. 1. (a) An idealized view of a hairy-rod solution. (b) A scheme of hairy-rod membranes in a solution. In both cases a simplified 2-dimensional picture is drawn with the rods being perpendicular to the drawing plane.

In order to proceed the approach developed in Refs.[28, 29] is employed to estimate the rod-solvent interaction free energy as

$$\frac{F_{RS}^{(sol)}}{N_{tot}} = 2Ld\gamma_{RA}\nu_0 c^{(sol)}, \tag{3}$$

where the "interfacial" energy parameter $\gamma_{RS}$ is used to describe the interaction between backbone monomers and solvent[28]. $L$ and $d$ are the length and the diameter of the backbone rod, $N_{tot}$ is the total number of molecules in the system, $\nu_0$ the monomeric volume, and $c^{(sol)}$ the concentration of the solvent molecules in the vicinity of the backbone. Using the same arguments we get

$$\frac{F_{RA}^{(sol)}}{N_{tot}} 2Ld\gamma_{RA}\nu_0 c_2, \tag{4}$$

where $c_2$ is the concentration of the alkyl monomers around the backbone so that $\nu_0\left(c_2^{(sol)} + c_2\right) \equiv 1$. In the formulas above some numerical constants of the order of unity have been omitted. The last term in the Eq. (1) accounts for the translational entropy and has the same form as in the Flory type theories

$$F_{tr}^{(sol)} = k_B T N_{tot}\left[\ln\frac{f}{e} + \frac{1-f}{\nu_0 f}\left(\frac{\pi d^2 L}{4} + \frac{\nu_0 NL}{b}\right)\ln\frac{1-f}{e}\right], \quad (5)$$

where $f$ is the volume fraction of the polymer in the system. Finally, the free energy of the isotropic solution phase, Equation (1) takes the form

$$\frac{F^{(sol)}}{N_{tot}k_B T} = \frac{L}{b}\left(\frac{\nu N}{a^2 b}\right) + 2Ld\left[\frac{\gamma_{RS}}{k_B T}\left(1-\nu_0 c_2\right) + \frac{\gamma_{RA}}{k_B T}\nu_0 c_2\right] + \ln\frac{f}{e} + \frac{1-f}{v_0 f}\left(\frac{\pi d^2 L}{4} + \frac{\nu_0 NL}{b}\right)\ln\frac{1-f}{e}, \quad (6)$$

with $c_2 = \left(a^2 b^2 d^2 \nu\right)^{-1/3}$ calculated based on the formulas given in Ref. [27].

The free energy of other competing phase, the solution with membranes, can be calculated along the same lines which yield

$$\frac{F^{(mem)}}{N_{tot}k_B T} = \frac{2NL}{b}\left(\frac{\nu}{abd}\right)^{2/3} + Ld\left[\frac{\gamma_{RS}}{k_B T}\left(1-\nu_0 c_1\right) + \frac{\gamma_{RA}}{k_B T}\nu_0 c_1\right] + \frac{1-f}{v_0 f}\left(\frac{\pi d^2 L}{4} + \frac{\nu_0 NL}{b}\right)\ln\frac{1-f}{e}. \quad (7)$$

where $c_1 = \nu^{-1/3}\left(abd\right)^{-2/3}$ is the concentration of the alkyl monomers around a double layered sheet of backbones. We also made use of $F_1^{(mem)} = 2N\left(\nu/\left(abd\right)\right)^{2/3}$ for the planar brush free energy per chain[30]. The interaction free energy is corrected by the fact that only a half of the surface area of the rods is in contact with solvent or side chains (cf., Fig. 1).

### B. Rod-sheet transition

The free energies lead to an estimation of the isotropic solution - membranes transition temperature $T_{mem}$*. By equating Eqs. (6) and (7) we get

$$\frac{1}{k_B T_{mem}^*} = \frac{2\left(\nu/abd\right)^{2/3} N - \left(\nu/a^2 b\right)^{1/2}\sqrt{N} - \left(b/L\right)\ln\left(f/e\right)}{bd\left[\gamma_{RS} + \left(\gamma_{RA} - \gamma_{RS}\right)\nu_0\left(2c_2 - c_1\right)\right]}. \quad (8)$$

It is assumed above that $\nu$, $\gamma_{RA}$, and $\gamma_{RS}$ do not depend on the temperature. Although generally incorrect, these assumptions do not change the scaling behavior of $T_{mem}$*. Another important point is that the Eq. (8) is valid for relatively long side chains, at least so long that the distance between their grafting points is smaller than their Flory radius $R_F = a\left(\nu/a^3\right)^{1/5} N^{3/5}$, i.e., $N > N^* = \left(b/a\right)^{5/3}\left(\nu/a^3\right)^{1/3}$. For shorter side chains one can expect a picture where isotropic liquid demixes with decreasing temperature[19].

### C. Polymer-solvent demixing

We have so far ignored the polymer-solvent demixing. Without addressing it in detail we note that for long enough side chains demixing can give rise to a melt phase (with lamellar morphology) and virtually pure solvent. The free energy after demixing will be of the order of

$$\frac{F^{(demix)}}{N_{tot}k_BT} = \frac{3NL}{2b}\left(\frac{\nu}{abd}\right)^2 + Ld\frac{\gamma_{RA}}{k_BT}, \qquad (9)$$

where $F_1^{(lam)} = 3/2\, k_BTN\left(\nu_0/\left(abd\right)\right)^2$ is the elastic energy per side chain (see Ref.[28] for details). The free energy, Eq. (9), scales in the same way as that of the membrane phase, Eq. (7), which implies that either the regime of thermodynamic stability of membranes is quite narrow or they are thermodynamically unstable.

### D. Phase diagram

Overall, the solution membranes and isotropic-nematic transition temperatures are predicted by Eqs. (8) and (9). This result is illustrated in Fig. 2.

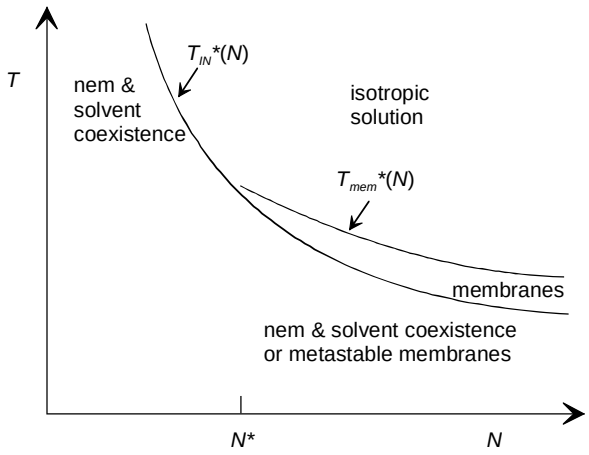


FIG. 2. The schematical presentation of transition temperatures, $T_{IN}*(N)$ and $T_{mem}*(N)$ ,as a function of side chain length $N$ . For long side chains, membranes can appear as an intermediate step between isotropic solution and demixed state. The demixing temperature $T_{IN}*(N)$, here shown schematically, has been calculated in Ref. [19].

## III. EXPERIMENT

### A. Materials

The chemical structures of used PFs are shown in Fig. 3. PF6, with the number averaged molecular weight ($M_n$)=84 kg/mol, and the weight averaged molecular weight ($M_w$)=200 kg/mol), PF7 ($M_n$=63 kg/mol, $M_w$=144 kg/mol), poly(9,9-dioctylfluorene), PF8 ($M_n$=48 kg/mol, $M_w$=132 kg/mol), poly(9,9-dinonylfluorene), PF9 ($M_n$=109 kg/mol, $M_w$=221 kg/mol), and poly(9,9-didecylfluorene), and PF10 ($M_n$=86 kg/mol, $M_w$=236 kg/mol) were prepared following the Yamamoto-type polymerization with $Ni(COD)_2$ catalyst[5]. Poly(9,9-dioctylfluorene)/(9,9-bis-(2-ethylhexyl)-fluorene) random copolymers (or F8-F2/6) ($M_n$ >>5 kg/mol) and poly(9,9-bis-(2-ethylhexyl)-fluorene)/(9,9-bis-fluorenone) random copolymer (or F2/6-fluorenone) were prepared similarly but

starting from the corresponding dibromofluorene monomers[31]. The applied stoichiometric weight fractions of 9,9-dialkylfluorene (F8) and 2-ethylhexylfluorene (F2/6) units were 95:5 (a corresponding polymer denoted as $F8_{0.95}$-$F2/6_{0.05}$), 90:10 ($F8_{0.90}$-$F2/6_{0.10}$), and 50:50 ($F8_{0.50}$-$F2/6_{0.50}$). For F2/6-fluorenone the proportion of 2-ethylhexylfluorene units to fluorenone units was 95:5 (the polymer denoted as $F2/6_{0.95}$-$fluorenone_{0.05}$).

The PFs were dissolved either in 10 mg/mL MCH (Sigma-Aldrich) or deuterated methylcyclohexane (MCH-$d_{14}$) (99.5 % D, Apollo Scientific Ltd). MCH-$d_{14}$ was employed in the case of neutron scattering, whereas MCH was used otherwise. Only PF10 is soluble in MCH at room temperature at the applied concentration. Therefore, for neutron scattering, the solutions of all polymers except PF6 were first heated up to 80-85 $^{o}$C and stirred for 5-10 minutes until completely clear solutions were observed. These samples were then cooled from 80-85 $^{o}$C down to -25 $^{o}$C for 30 minutes and subsequently warmed to 20 $^{o}$C before measurements. PF6 solution was prepared similarly but was heated up to 100 $^{o}$C, a temperature limited by the boiling point of MCH (101 $^{o}$C). PF6/MCH, PF7/MCH, PF8/MCH, PF9/MCH, $F8_{0.95}$-$F2/6_{0.05}$/MCH, and $F8_{0.90}$-$F2/6_{0.10}$/MCH systems are viscous or gel-like at 20 $^{o}$C while other mixtures appear as transparent liquids. PF6/MCH is not transparent even at 100 $^{o}$C. The small-angle neutron scattering (SANS) measurements were made immediately after sample preparation at two constant temperatures. Small- and wide-angle X-ray scattering (SAXS/WAXS) measurements and differential scanning calorimetry (DSC) were used to monitor the thermal process *in-situ*. No significant macrophase separation was observed during the measurements (over a few hours).

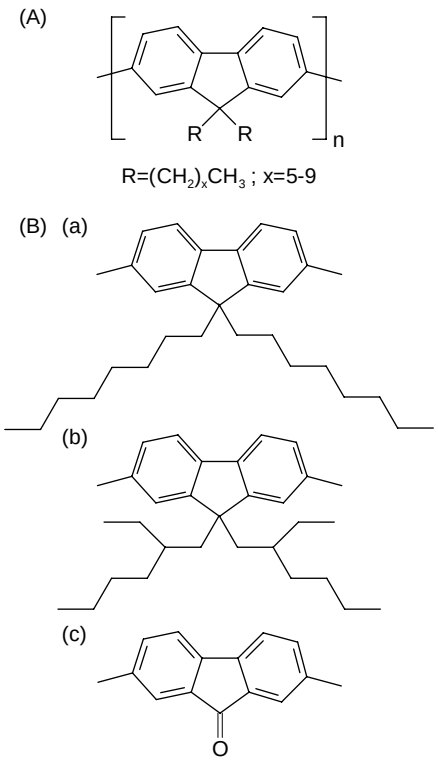


FIG. 3. (A) Chemical structure of PFs studied as a function of side chain length. The side chain length varied from 6 to 10 beds. (B) Chemical structure of random copolymers constituting different degree of side chain branching. In this case F8, (a), and F2/6 monomers, (b), were mixed with the molar ratios of 95:5, 90:10, and 50:50. Additionally F2/6 (b) was mixed with 9,9-bis-fluorenone units, (c), with the ratio of 90:10.

### B. Small-angle neutron scattering

SANS measurements were performed using the SANS-1 instrument at the GKSS Research Centre in Geesthacht, Germany[32]. Several sample-to-detector distances (from 0.7 to 9.7 m) and wavelength from 5 to 12 Å were employed to cover the $q$-range from 0.004 to 0.25 $Å^{-1}$. The samples were filled in Hellma quartz cells of 2 mm path length. The temperature was controlled by Julabo thermostat. The raw scattering patterns were corrected for sample transmission and air sample cell scattering by conventional

procedures[33]. The isotropic 2D scattering patterns were azimuthally averaged, converted to an absolute scale and corrected for detector efficiency dividing by the incoherent scattering spectra of 1 mm thick pure water. The scattering from MCH-$d_{14}$ used for the sample preparation was subtracted as a background. The small incoherent scattering due to the non-deuterated polymer is taken into account in fitting procedures. The data for each sample was collected for 6 hours on average.

### C. Small-angle and wide-angle X-ray scattering

SAXS/WAXS measurements were carried out using a sealed tube based pinhole camera. The radiation ($CuK_\alpha$, $\lambda$=1.54 Å) was monochromatized with multilayer mirrors (Montel Optics by Incoatec), whereafter the double bounced beam was selected with slits and collimated to the size 0.5 mm × 0.5 mm. The scattering patterns were measured using HI-STAR multi-wire proportional counter (Bruker AXS). The sample detector distance was 170 mm and the covered *q*-range from 0.05 to 1.3 $Å^{-1}$. The transmitted flux was monitored during the measurement through the transparent beam stop, a 3 mm disc press-cut from 0.25 mm thick copper foil. The samples were measured in flat sample holders with 1 mm path length and 6 μm thick mylar windows[34]. The temperature was controlled using Linkam TP93 hot stage and liquid nitrogen. The background depends on the temperature and was subtracted for each temperature separately. The intensity was normalized to electron scattering units per unit volume using water as a primary standard. $I(0)$ is 0.208 electrons/$Å^3$ for water.

The samples were prepared as described above, by dissolving in MCH on a hot plate. Then they were transferred with a syringe rapidly to the preheated sample holders, sealed with epoxy, and measured at 80 $^oC$ for 15 min to check whether they are dissolved to the

molecular level. Thereafter they were quenched in approximately 1 min to -12 $^{o}$C, measured (and kept) there for 30 min and heated slowly (0.1 $^{o}$C/min) back to 80 $^{o}$C while measuring. An exception was PF10/MCH which was dissolved at 30 $^{o}$C, quenched at -100 $^{o}$C, and heated 0.5 $^{o}$C/min.

### D. Differential scanning calorimetry

DSC measurements were performed using a Perkin-Elmer Pyris 1 DSC under a nitrogen environment. After the first heating-cooling (85- -25 $^{o}$C) cycle the samples were cooled from room temperature down to the - 25 $^{o}$C for 30 minutes and heated again up to the 85 $^{o}$C. The scanning rate was 5 $^{o}$C/min and the sample size ca. 10 mg.

## IV. DATA ANALYSIS

### A. Analysis of neutron scattering

The SANS patterns were first qualitatively analyzed by comparison of absolute intensities, shape of curves and the determination of the slope. The scattering cross section data can be approximated by simple power law dependence as

$$\frac{d\Sigma(q)}{d\Omega} \sim q^{-\alpha}, \qquad (10)$$

where the obtained value of $\alpha$ obtained reflects the likely shape of aggregates in the solution on the studied length scale. If the exponent $\alpha$ is 1, this points to the rodlike objects. If $\alpha$ is slightly larger than 2 then the particles can be sheetlike. The scattering curves from all samples followed either one of two types of exponential behaviors. These observations allowed the further analysis of the scattering data by applying the Indirect Fourier Transformation Method (IFT)[35] with rodlike and sheetlike shapes of particles.

In the IFT analysis the scattering intensities are expressed via the pair distance distribution function.

The scattering intensities of cylindrical particles are related to the pair distance distribution function of cylindrical cross section, $\tilde{p}_{\mathrm{CS}}(r)$, as

$$\frac{\mathrm{d}\Sigma(q)}{\mathrm{d}\Omega}\frac{1}{c}=\left(\frac{\pi}{q}\right)2\pi\int_0^\infty \tilde{p}_{\mathrm{CS}}(r)J_0(qr)rdr=\left(\frac{\pi}{q}\right)I_{\mathrm{CS}}(q), \tag{11}$$

where $J_0$ is the zeroth-order Bessel function and $I_{\mathrm{CS}}(q)$ is the cross-sectional scattering intensity.

For sheetlike particles the scattering intensity is related to the pair distance distribution function of thickness, $\tilde{p}_{\mathrm{T}}(r)$, as

$$\frac{\mathrm{d}\Sigma(q)}{\mathrm{d}\Omega}\frac{1}{c}=\left(\frac{2\pi}{q^2}\right)\pi\int_0^\infty \tilde{p}_{\mathrm{T}}(r)\cos(qr)dr=\left(\frac{2\pi}{q^2}\right)I_{\mathrm{T}}(q), \tag{12}$$

where $I_{\mathrm{T}}(q)$ is the thickness scattering function.

From the pair distance distribution functions, the mass of aggregates (mass per unit length or unit area) and the radius of gyration can be obtained. The latter is associated with the distribution of scattering length density, and with certain assumptions this distribution can be transformed to thickness $(T)$ or radius of cross section $(R_{CS})$.

### B. Analysis of X-ray scattering

The clear-cut data allowed us to use idealized models for SAXS as described in Ref.[36]. As a starting point, we describe the dissolved hairy-rod polymers and the sheets as stiff cylinders. Their scattering intensity is given as

$$I(q,\theta)=\left[2\frac{J_1(qR\sin\theta)}{qR\sin\theta}j_0\left(\frac{qL\cos\theta}{2}\right)\right]^2, \tag{13}$$

where $\theta$ is the angle between $q$-vector and cylinder axis. $L$ is the length and $R$ the radius of the cylinder. The two Bessel functions in Eq. (13) are defined as

$$J_1(x)=\frac{1}{2\pi}\int_0^{2\pi}\exp\left[i(x\sin\theta-\theta)\right]d\theta, \tag{14}$$

and

$$j_0(x)=\frac{\sin x}{x}. \tag{15}$$

The angular averaged scattering intensity is obtained by numerical integration over $\theta$. For the rodlike polymers $(R\ll L)$ the scattering curve $I(q)$ follows the power law $I(q)\sim q^{-1}$ for $1/L<q<1/R$. This slope levels off at low angles $q<L^{-1}$ to the Guinier law regime, whereas at $q>R^{-1}$ it has a downturn corresponding to the cross-sectional scattering $qI(q)\sim\exp\left(-q^2R^2/4\right)$ and, finally, to the Porod slope $I(q)\sim q^{-4}$. Similar arguments can be used for the sheetlike particles with the relative magnitudes of $R$ and $L$ interchanged. In this case the intermediate slope $\sim q^{-2}$ is obtained for $1/R<q<1/L$.

For these anisotropic extremities the essential form of the intensities may be reduced to the Ornstein-Zernike type scattering factors[20] as

$$S(q)=\frac{1}{1+qL\exp\left(q^2R^2/4\right)}, \tag{16}$$

for the rods and

$$S(q)=\frac{1}{1+(qR)^2\exp\left(q^2L^2/12\right)}, \tag{17}$$

for the sheets. In these Equations $L$ and $R$, respectively indicate the upper limit of validities where the particles still can be regarded as individual rods or sheets.

Of interest here is the power law behavior $I(q) \sim q^{-1}$ or $\sim q^{-2}$. It can be shown[37] that the intensities from a single rod or sheet take, respectively, the form

$$I_1(q) = LA^2(\Delta\rho)^2 \frac{\pi}{q} = Z_{tot}^2 \frac{\pi}{qL}, \tag{18}$$

for the rods and

$$I_1(q) = AL^2(\Delta\rho)^2 \frac{2\pi}{q^2} = Z_{tot}^2 \frac{2\pi}{q^2 A}, \tag{19}$$

for the sheets. $A$ is the area of the cross section, $\Delta\rho$ the scattering contrast, and $Z_{tot}$ the effective number of scattering electrons in the chain as a whole.

Next we calculate the volume of normalized intensity for hairy-rods dissolved to concentration $c$ (expressed in mass/volume) as

$$i(q) = nI_1(q), \tag{20}$$

where $n = cN_A\rho_l^2/M_l$ is the number density. The intensities are proportional to concentrations and depend on the specific properties of polymers through

$$q \cdot i(q) = c \cdot \pi N_A \rho_l^2 / M_l, \tag{21}$$

for the rods and

$$q^2 \cdot i(q) = c \cdot 2\pi N_A \rho_s^2 / M_s, \tag{22}$$

for the sheets. Here $M_l$ and $\rho_l$ are, respectively, the molar mass and scattering amplitude (number of electrons) per unit length whereas $M_A$ and $\rho_A$ are the molar mass and scattering amplitude per unit area. The asymptotic forms of Eqs. (21) and (22) do not depend explicitly on the length of rods or size of sheets and are valid even for flexible

polymers or sheets. When the rods are assumed to be single polymer chains $M_l$ and $\rho_l$ can be estimated from the bulk properties of polymer and solvent. The values calculated in that way for PFn/MCH systems are given in Table I.

TABLE I. Parameters for linear side chain PFs: $\rho$ is density, $\rho_e$ electron density, $M_l$ molar mass per unit volume, and $\rho_l$ scattering amplitude per unit length in MCH solvent. The concentration is 10 mg/mL.

| Material | $\rho$ (e/Å$^3$) | $\rho_e$ (e/Å$^3$) | $M_l$ (g/molÅ) | $\rho_l$ (e/Å$^3$) |
|---|---|---|---|---|
| PF6 | 1.054 | 0.348 | 40.0 | 5.22 |
| PF7 | 1.035 | 0.343 | 43.4 | 5.42 |
| PF8 | 1.020 | 0.339 | 46.7 | 5.61 |
| PF9 | 1007 | 0.335 | 50.1 | 5.81 |
| PF10 | 0.996 | 0.332 | 53.5 | 6.01 |
| MCH | 0.77 | 0.265 | n/a | n/a |

If the polymers self-organize (e.g., in sheetlike membranes) further assumptions concerning the packing density are needed. The density can be calculated in a converse fashion as the properties of single polymers are known. As discussed in the Section II, we presume a transition of rods into sheetlike membranes. Let $d_s$ be the average lateral distance of the polymers in the sheets and assume that the other factors remain constant, we obtain $\rho_s = \rho_l / d_s$ and $M_s = M_l / d_s$. The ratio of two asymptotes is then

$$\frac{\lim_{q\to 0} q^2 i_{sheet}}{\lim_{q\to 0} q^2 i_{rod}} = \frac{2}{d_s}. \tag{23}$$

In other words, the crossover point of the intensity curves $i_{sheet}$ and $i_{rod}$ gives directly the packing density at $q = 2/d_s$. As the phase transition takes place as a function of temperature, the change in the scattering contrast has to be corrected with regard to temperature. However, inasmuch as we are dealing with two distinct phases that yield the same intensity per unit mass at the special point, a total transition between the phases is not essential, in analogy with the isobastic point known in spectroscopy.

A polymer in dilute solution may also show a crossover from rodlike form to Gaussian (random walk) form for which the scattering scales as $q^{-2}$ for $q < 2\pi / \xi$, where $\xi$ is the Kuhn segment. A polymer in a dense solution or gel may contain large scale density fluctuations which result in a $q^{-4}$ upturn at small angles. These alternatives should be easily distinguished from the above forms by considering where the particular power law regimens appear in comparison with the experimental data of the structures.

The overall idea of scattering powers is illustrated in Fig. 4. While a mixture of rods and sheets might be mistaken as Gaussian coils, for example, the crossover point between -2 and -1 behavior should occur at very low angles and an extensive -2 region at very low concentration due to the scarcity of such random walk chains. In the present work the clear-cut thermal behavior alone will refute the notion of Gaussian coils.

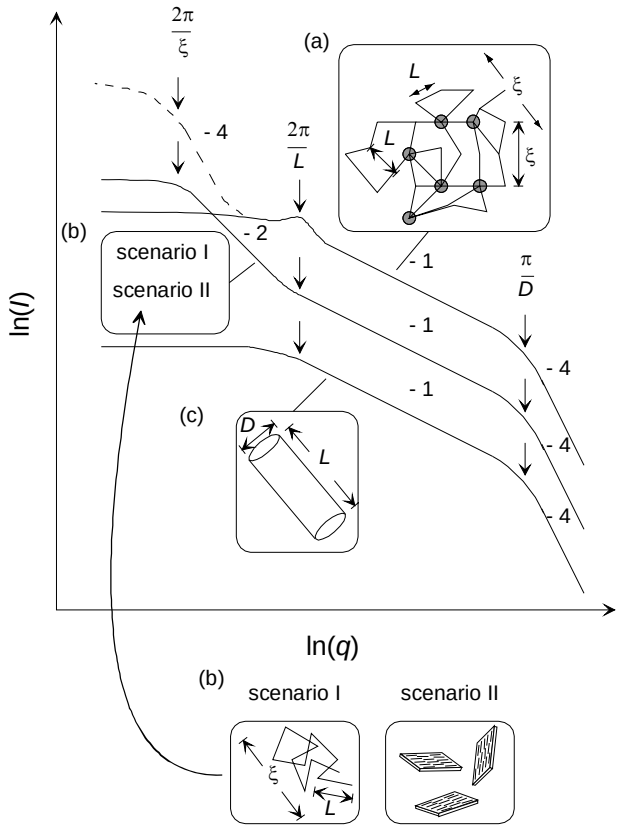


FIG. 4. An idealized description of the small-angle scattering data and proposed solution structures of hairy-rod PFs. (a) A network-like structure with cross-linked nodes, (b) a structure of rodlike particles forming Gaussian coils (scenario I) or sheetlike membranes (scenario II) in the longer length scales, and (c) a structure of fully dissolved rodlike particles (essentially single polymer chains).

## V. RESULTS AND DISCUSSION

### A. Solution structure as a function of side chain length

The influence of the side chain length on the solution structure of linear side chain PFs in MCH at room temperature has been described in our previous work[12]. In general terms PF6, PF7, PF8, and PF9 show sheetlike aggregates MCH whereas PF10 dissolves down to the molecular level. These sheets show an odd-even effect so that PF7/MCH and PF9/MCH sheets are thicker but laterally smaller than those of PF6/MCH and PF8/MCH. We have also found that the internal details of the sheets depend on the side chain length in complicated manner. In brief, relatively sharp reflections at $q$=0.60 Å$^{-1}$, $q$=0.48 Å$^{-1}$, and $q$=0.43 Å$^{-1}$, respectively, are seen for PF6/MCH, PF8/MCH, and PF9/MCH with accompanying peaks at the wide angles. Moreover, PF7/MCH, PF8/MCH, and PF9/MCH contain a conformational isomer $C_\beta$[12]. This picture is, however, limited to the room temperature. Hereafter, the intermolecular nanometer scale assemblies are presented in a wide temperature range.

Figs. 5 and 6, respectively, show examples of SAXS data of PF/MCH mixtures with odd and even numbered side chains as a function of temperature. At the room temperature, the data show similar solution structures as reported earlier[12]. A sharp visual transition from gel to liquid is seen when heating them from -25 $^o$C to 85 $^o$C. This transition corresponds to the sudden chance in the SAXS data essentially from -2 decay to -1 decay. This alteration indicates the structural order-disorder transition from sheetlike structures to fully dissolved rodlike chains. The length of the polymer is not seen in the SAXS data but the downturn at low angles is likely due to the concentration effects (polymer-polymer interference) and/or onset of larger scale morphology (e.g.

cross links or branching). The wider angles reveal in turn a Bragg reflection at around 0.5 $Å^{-1}$ its strength and exact location depending on the polymer. This maximum refers to the mesomorphic $\beta$ phase its known for solid state PF8[22] and PF6[38].

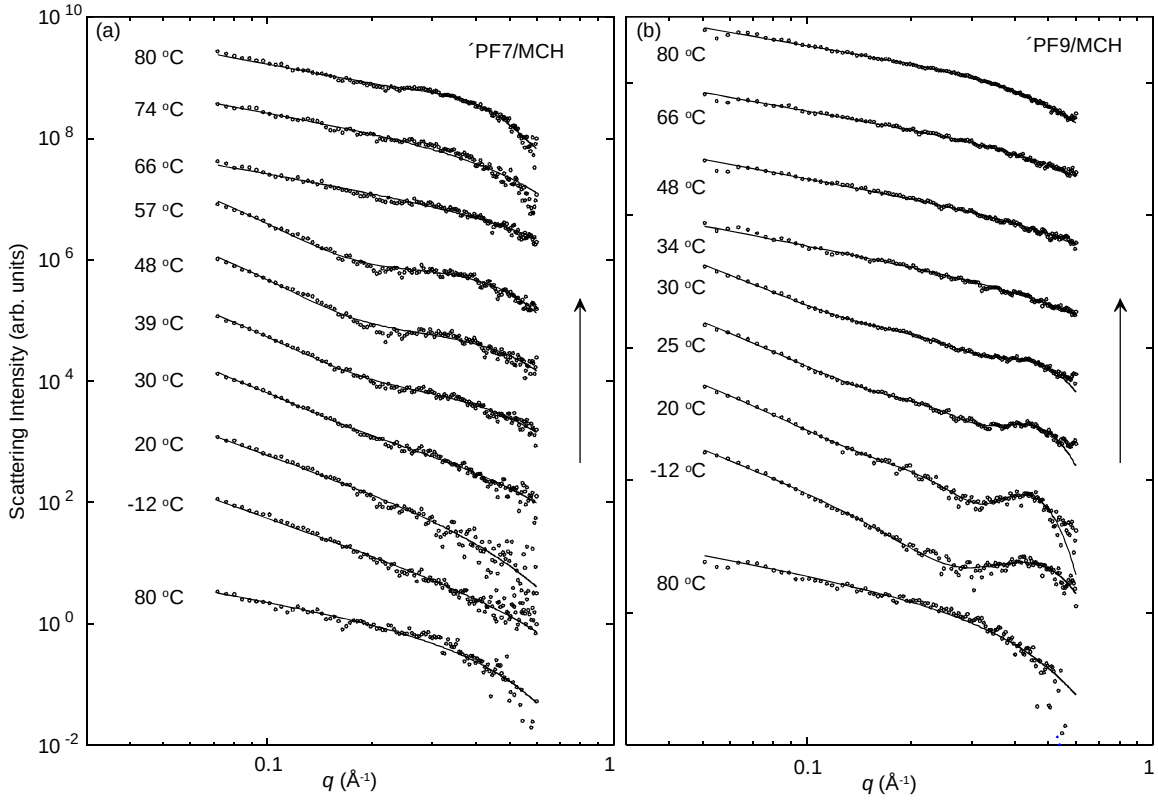


FIG. 5. Open circles present selected SAXS data of PF7/MCH (a) and PF9/MCH (b), during very slow heating (0.1 °C/min) after a heating-cooling cycle from 80 °C to -12 °C. Solid lines correspond to the model described in Section IV. For PF7/MCH curves corresponding temperatures below 60 °C follow $q^{-2}$ slope whereas this is true for PF9/MCH below 31 °C. The concentrations were 10 mg/mL

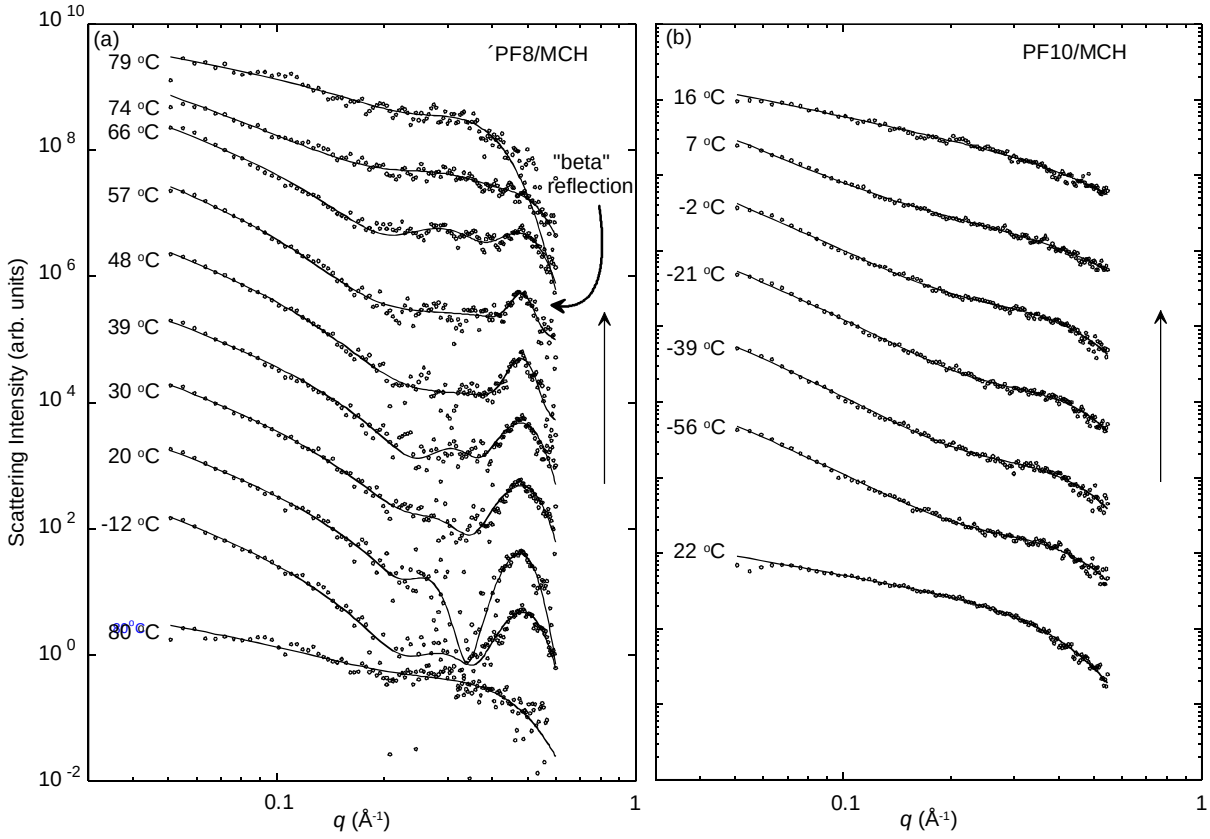


FIG. 6. Selected SAXS data of PF8/MCH (a) and PF10MCH (b) during heating (0.1 $^{o}$C/min); after a heating-cooling cycle from 80 $^{o}$C to -12 $^{o}$C. A distinctive "beta" maximum is present for PF8/MCH at 0.46 Å$^{-1}$. The concentration was 10 mg/mL

In Fig. 7 we plot characteristic SAXS/WAXS curves for all systems below and above this transition. An exception is PF6/MCH which shows -2 decay but no clear phase transition. Moreover, it is likely that PF6/MCH system is to certain extent macrophase separated as indicated by strong light scattering. In this rather high concentration its solution structure is interpreted as lyotropic liquid crystal and surplus solvent. A beta reflection 200[12] is visible to varying degree. The radii of the rods and thicknesses of the sheets as determined by SAXS and WAXS data are compiled in Table II.

Interestingly, the sheet thicknesses are equivalent to two polymer layers. This justifies the idea of double layer membrane, an assumption made in Section II.

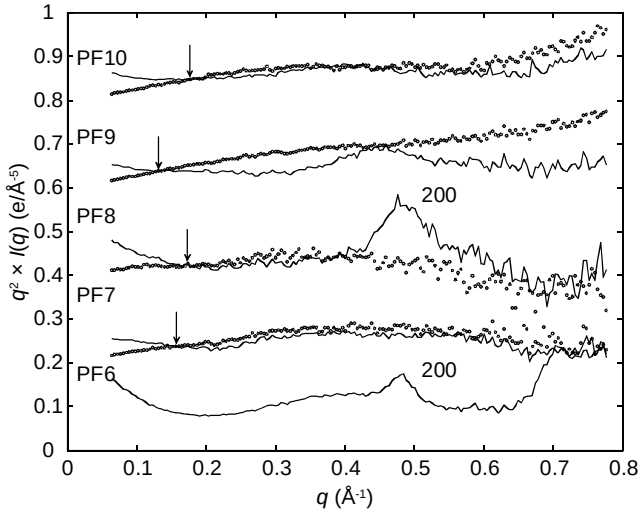


FIG. 7. The SAXS/WAXS data multiplied by $q^2$ of linear side chain PF/MCH mixtures. Solid lines represent the situation below and dotted lines above the membrane-isotropic phase transition. The arrows mark the crossing points of -1 and -2 slopes.

TABLE II. Various parameters characterizing the thicknesses of the sheets of linear side chain PFs in 10 mg/mL MCH as determined by SAXS: $R$ has been obtained from fitting Eq. (17), $d_\beta$ from the sharp "beta" maximum, and $d_s$ from the crossing point of the data.

| Material | $R$ (Å) | $d_\beta$ (Å) | $d_s$ (Å) |
|---|---|---|---|
| PF6 | n/a | 13.1 | n/a |
| PF7 | 3.9 | n/a | 12 |
| PF8 | n/a | 13.1 | 11 |
| PF9 | 3.9 | 13.7 | 15 |
| PF10 | 4.4 | n/a | 11 |

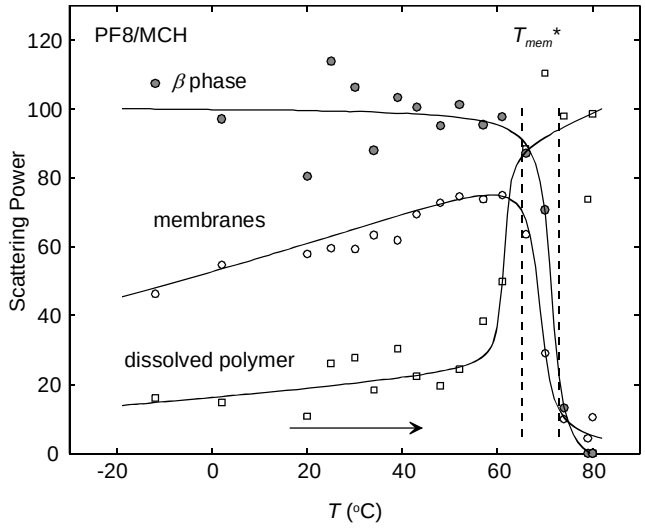


FIG. 8. Estimated scattering powers of the $\beta$ phase (solid circles), loose sheetlike membranes (open circles), and dissolved rodlike polymers (open squares) in PF8/MCH system on heating. The solid lines are the best fits to the data. The order-disorder transition is marked by the vertical dotted lines. The $\beta$ phase is located within the membranes and can be distinguished from the loose membrane by a Bragg reflection.

Overall, we interpret that the experimentally observed lyotropic-membrane and membrane isotropic phase transitions are equivalent to the $N^*$ and $T_{mem}^*$ concepts predicted by theory. These results set the ground on the phase behavior of PF/MCH system. Furthermore, considering SAXS/WAXS data combined with the previous findings in optical spectroscopy[12], we are able to identify three distinct material fractions present in the membrane phase. Firstly, the 2-dimensional aggregates primarily consist of loose membranes generally leading to the $q^{-2}$ scaling. Secondly, they contain a fraction of well packed $\beta$ sheets which lead to the Bragg reflection at around 0.46 Å$^{-1}$. This part of the membrane also leads to the optical features of the conformational isomer $C_\beta$, a picture initially put forward in our previous paper[12]. Thirdly, the samples contain

small fraction of the fully dissolved rods being responsible for the -1 contribution in the SAXS data. Fig. 8, then, presents scattering powers of these material fractions as developed as a function of temperature for PF8/MCH. The scattering powers cannot be understood as exact materials fractions except for isotropic phase for $T > T_{mem}$*.

### B. Solution structure as a function of side chain branching

As the case $N = 8$ represents a magic number when maximizing the amount of $C_\beta$ isomer in PF/MCH system[12], it deserves more attention. We have previously shown that while PF8/MCH organizes into the membranes at the room temperature the system composed by a branched side chain PF2/6 forms only an isotropic phase[10]. PF2/6 and PF8 have the same amount of side chain beds they differing only in terms of side chain branching (cf., Fig. 3). The other factors influencing phase behavior are constant. In order to study the solution structure as a function of side chain branching for $N = 8$ further, we synthesized F2/$6_{0.95}$-fluorenone$_{0.05}$ random copolymers and varied the fraction of F8 and F2/6 monomers from one extreme to another. A PF2/6 with fluorenone units (or F2/$6_{0.95}$-fluorenone$_{0.05}$) was used for comparison. Fluorenones represent keto defects arising from PF oxidation[38, 16] and this latter experiment mirrors whether 5% oxidation influences the PF solution structure in MCH. We note that this copolymer represents serious oxidation and already 0.1% oxidation level is optically pronounced[38].

On the mixing and heating-cooling cycle $F8_{0.95}$-F2/$6_{0.05}$/MCH and $F8_{0.90}$-F2/$6_{0.10}$/MCH form viscous gels resembling PF8/MCH whereas $F8_{0.50}$-F2/$6_{0.50}$/MCH and F2/$6_{0.95}$-fluorenone$_{0.05}$/MCH remain clear liquids akin to PF2/6/MCH. Fig. 9 plots SANS data of the copolymers studied after the heating-cooling cycle at 20 $^{o}$C. The data of $F8_{0.95}$-

F2/$6_{0.05}$/MCH and F$8_{0.90}$-F2/$6_{0.10}$/MCH differ clearly from those of F$8_{0.50}$-F2/$6_{0.50}$ /MCH and F2/$6_{0.95}$-fluorenone$_{0.05}$ /MCH. The former show a distinctive -2 decay and the latter follow -1 slope. These observations point to the membrane and isotropic phases likening PF8/MCH and PF2/6/MCH. Note that the intensity curves cross at the high $q$ which implies that most of material must be in one single phase. This means that any difference between the solution structure of F$8_{0.90}$-F2/$6_{0.10}$/MCH and PF8/MCH is subtle.

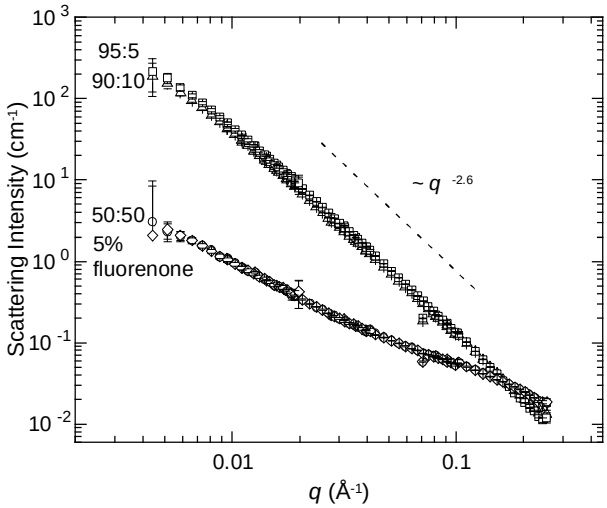


FIG. 9. SANS data of F$8_{0.95}$-F2/$6_{0.05}$ (open squares), F$8_{0.90}$-F2/$6_{0.10}$ (open triangles), F$8_{0.50}$-F2/$6_{0.50}$ (solid circles), and F2/$6_{0.95}$-fluorenone$_{0.05}$ (open diamonds) in 10 mg/mL MCH-$d_{14}$ at 20.0 $^{o}$C±0.5. The dashed line shows the -2.6 decay for comparison.

When the F$8_{0.95}$-F2/$6_{0.05}$/MCH and F$8_{0.90}$-F2/$6_{0.10}$/MCH mixtures showing the existence of 2-dimensional structure at room temperature are heated (up to 85 $^{o}$C), they undergone a visual phase transition to transparent fluid. The obvious question is whether this affects the structure in the same way as in PF8/MCH. Fig. 10 plots SANS data of these samples at 84 $^{o}$C. Corresponding data of PF8/MCH are shown for comparison. All data confirm a distinctive -1 decay indicating a phase transition from the membrane phase to the fully dissolved rods. These characteristics allowed us to fit the data to models of cylindrical or

sheetlike particles. The essential structural parameters so obtained are compiled in Table III. The thicknesses of sheets correspond to two polymer layers. Thus the experiment is commensurate with the theory based on an idea of a double layer membrane.

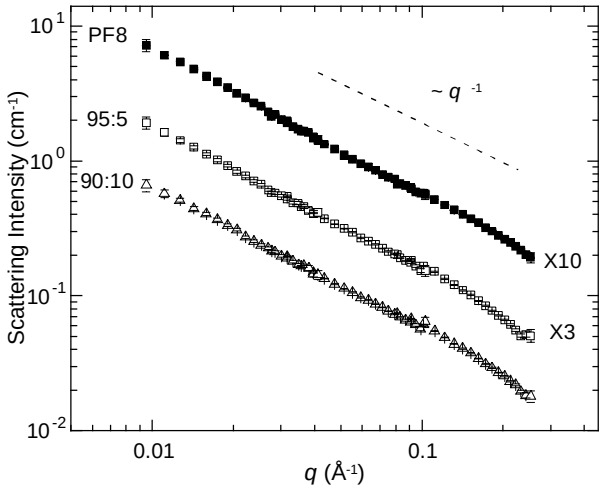


FIG. 10. SANS data of PF8 (solid squares), $F8_{0.95}$-$F2/6_{0.05}$ (open squares), and $F8_{0.90}$-$F2/6_{0.10}$ (open triangles) in MCH-$d_{14}$ at 84 $^{o}$C±1. The two latter data are shifted for clarity. The dashed line shows the -1 decay for comparison. The concentrations were 10 mg/mL

TABLE III. Various parameters characterizing the structures of PF copolymers in 10 mg/mL MCH as determined by SANS:

| Polymer in MCH | Temperature ($^{o}$C) | Model | Analyzed $q$-range (Å) | $D_{max}$ (Å) | $R_{CS,g}$ (Å) | $R_{Tg}$ (Å) |
|---|---|---|---|---|---|---|
| $F8_{0.95}$-$F2/6_{0.05}$ | 20.0±0.5 | cylinder | 0.03-0.3 | 50±6 | 12.8±0.6 | n/a |
| $F8_{0.90}$-$F2/6_{0.10}$ | 20.0±0.5 | sheet | 0.004-0.3 | ~30 | n/a | 8.8±0.2 |
| $F8_{0.50}$-$F2/6_{0.50}$ | 20.0±0.5 | sheet | 0.004-0.3 | ~30 | n/a | 8.7±0.2 |
| $F8_{0.90}$-$F2/6_{0.10}$ | 84±1 | cylinder | 0.03-0.3 | 50±6 | 11.0±0.7 | n/a |
| $F8_{0.50}$-$F2/6_{0.50}$ | 84±1 | cylinder | 0.03-0.3 | 50±5 | 11.1±0.7 | n/a |
| PF8 | 84±1 | cylinder | 0.03-0.3 | 50±7 | 13.1±0.6 | n/a |

### C. Phase diagram

The exact transition temperature $T_{mem}$* was studied for all abovementioned systems in detail by SAXS and DSC. These results are compiled in Table IV. Fig. 11 plots the proposed experimental phase diagram. In the Section II we predict an intermediate membrane phase upon cooling of an isotropic hairy-rod solution this is indeed experimentally confirmed. Most importantly, the theoretically predicted scaling of $T_{mem}^{*}(N) \sim N^{-1/2}$ illustrated in Fig. 2 is in accord with that seen for $N \geq 8$ in Fig. 11. Several issues ought to be commented.

TABLE IV. Transition temperature $(T_{mem}^{*})$ for the membrane-isotropic phase transition of the PF samples in 10 mg/mL MCH as determined by the DSC and SAXS.

| Material | DSC $T_{mem}$* (ºC) | SAXS $T_{mem}$* (ºC) |
|---|---|---|
| PF6 | n/a | n/a |
| PF7 | not observed | 59±4 |
| PF8 | 65±2 | 70±1 |
| PF9 | not observed | 30±3 |
| PF10 | 13±2 | 7±5 |
| $F8_{0.95}$-$F2/6_{0.05}$ | 56±4 | 56±5 |
| $F8_{0.90}$-$F2/6_{0.10}$ | 50±2 | 48±6 |
| $F8_{0.50}$-$F2/6_{0.50}$ | not observed | not observed |

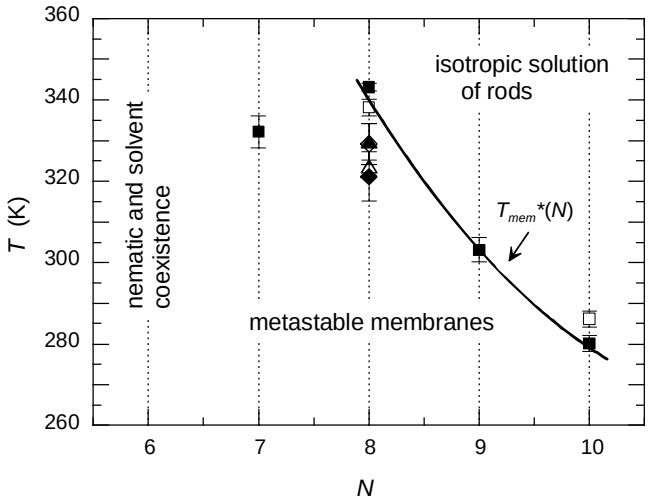


FIG. 11. The experimental phase diagram showing the membrane isotropic phase transition temperature of PFs, $T_{mem}$*, as a function of side chain length, $N$, based on SAXS (solid squares) and DSC (open squares) data. Also shown are corresponding transitions $T_{mem}^{*}(N=8)$ for $F8_{0.90}$-$F2/6_{0.10}$ (triangles) and $F8_{0.90}$-$F2/6_{0.10}$ (diamonds) random copolymers based on SAXS (solid symbols) and DSC (open symbols) data. The dotted lines correspond to the experimentally studied $N$. The solid line separating 2 phase regimes is a guide to eye. The theoretical counterpart is shown in Fig. 2.

Firstly, although the equations shown in Section II are interpreted as semi-quantitative rather than exact but the physics behind the solution-to-membranes transition is easily reasoned. Apparently, the free energy of the system includes two major contributions. The first one, the elastic energy of the "blurs" formed by the alkyl chains, is mainly of entropic of origin. The other, interaction between rods and a poor (for the backbones) solvent, has a significant enthalpic component. This means that at high temperatures when the entropy is dominating, the state with the lower stretching should be more advantageous. The hairy-rods are thus dissolved in the solvent because the elastic energy

of the side chains of such a cylindrical brush is apparently lower than that of a planar one (cf, Fig. 1). Lowering the temperature amplifies the enthalpic term responsible for the solvent-backbone interaction. Hence, at a certain point the system strives to reduce the backbone-solvent contact area in spite of the higher stretching of the side chains and membranes are formed. Upon further cooling the system macroscopically demixes in line with the earlier predictions[19]. It is expected that analogous *n*-alkanes would be dissolved in MCH[39]. The question remains whether $T_{mem}$* is related to the melting temperature of *n*-alkanes that increases with increasing $N$ [40]. We may argue that dissolution and melting of the side chains are entropically inverse phenomena and therefore opposite behavior seems logical.

Secondly, although not directly included in the model, a two branched side chain having $N$ monomers can be roughly seen as two $N/2$ chains with twice as high grafting density, i.e., a distance $b/2$ between the grafts. As follows from Eq. (8), $T_{mem}^* \sim b^{5/3}/N$ decreases in such a case. This qualitatively corresponds to the experimentally observed behavior.

Thirdly, the samples in the membrane phase are metastable, slow macrophase separation occurring in a few days after preparation. This separation is so slow and it does not infer the measurements. We expect that for the long side chains the membranes can survive for long times even in the phase regime where demixing should have had place. The free energy difference between memberanes and macrophase separated system is quite low and, if membranes are interconnected (as it is expected[12]), their restricted mobility will considerably slow down the process. Interestingly, the $\beta$ phase is generally understood as an intrinsically metastable state, intermediate between a solvent-induced

clathrate and the equilibrium crystalline order of the undiluted state[22]. The metastability in the solid state is in agreement with both the proposed theoretical model and the experimentally proposed $\beta$ phase in PF/MCH mixtures.

Fourth, in the theory (Eq. 1) the interaction between the hairy-rods is neglected, which is plausible assumption in a low concentration regime. The used concentration (10 mg/mL ~ 1 wt-%) should constitute an uncorrelated particle system and no concentration effect is seen, when the concentration is lowered down to 5 mg/mL[10]. However, it is shown elsewhere[20] that the PF aggregates can form larger, network like structures. We have furthermore proposed that the observed crystallites can act as nodes of the network which implies that PF/MCH sheets are interconnected. Therefore, the interaction assumption should be considered with care.

Fifth, the transition between membrane phase and isotropic rodlike polymers could also be understood as a gelation transition well known for *n*-alkanes[41] and for instance for poly(methyl methacrylate) in toluene[42]. The latter system shows a two-step thermoreversible gelation mechanism where a fast intramolecular conformational change is followed by an intermolecular association. The theory presented in Section II represents equilibrium statistical mechanics and therefore do not reflect the mechanism of the aggregation. PF/MCH system could yet be understood in similar terms but with a very large hysteresis.

We finally note that the phase transitions can be determined for all membrane systems by SAXS but they cannot be observed for PF7 and PF9 by DSC. Whether this relates to the odd-even sequence in sheet structures[12] remains an open question.

## VI. CONCLUSIONS

In conclusion, we have conducted a systematic experimental study on how the phase behavior of PFs is controlled by the side chain length and branching. This study is founded on the theoretical predictions. MCH has been used as a representative solvent. The lyotropic phase with solvent coexistence, the membrane phase, and the isotropic phase are found in solution with increasing side chain length, $N$. A lyotropic phase transition is seen at $N^* \sim 6$. The membrane phase turns into the isotropic phase of dissolved rodlike polymers when the temperature is increased up to the limit $T_{mem}^*(N = 7-10)$, decreasing with $N$ for $N \geq 8$. The polymer branching is found to decrease $T^*$, an effect which is in accord with the theoretical reasoning. Polymer demixing and two types of membranes are theoretically predicted. The membrane phase is found to consist of loose sheets of two polymer layers, well packed beta sheets and smaller amount of fully dissolved polymers. The change of these fractions is given as a function of temperature. These results give a solid insight to the tailoring solution assemblies of hairy-rod polyfluorenes.

## ACKNOWLEDGEMENTS

M.. K. thanks F. B. Dias of the University of Durham, L. Almásy of the Budapest Neutron Centre, H. D. Burrows of the University of Coimbra, and M. J. Winokur of the University of Wisconsin-Madison for discussions as well as European Commission for support (Contract n°: RII3-CT-2003-505925).

[1] A. Y. Grosberg and A. R. Khokhlov, *Statistical Physics of Macromolecules* (American Institute of Physics, Woodbury, NY, 1994).

[2] G. Wegner, Macrom. Chem. Phys. **204**, 347 (2003).

[3] M. J. Winokur, in *Handbook of Conducting Polymers*, edited by T. A. Skotheim and J. R. Reynolds (CRC Press LLC, Boca Raton, FL, 2007), Vol. 1, p. 1.

[4] D. Neher, Macromol. Rapid. Comm. **22**, 1365 (2001).

[5] U. Scherf and E. J. W. List, Adv. Mater. **14**, 477 (2002).

[6] A. C. Grimsdale and K. Müllen, Adv. Polym. Sci. **199**, 1 (2006).

[7] M. Knaapila, R. Stepanyan, B. P. Lyons, M. Torkkeli, and A. P. Monkman, Adv. Funct. Mater. **16**, 599 (2006).

[8] J. Zaumseil and H. Sirringhaus, Chem. Rev. **107**, 1296 (2007).

[9] M. Grell, D. D. C. Bradley, X. Long, T. Chamberlain, M. Inbasekaran, E. P. Woo, and M. Soliman, Acta Polym. **49**, 439 (1998).

[10] M. Knaapila, V. M. Garamus, F. B. Dias, L. Almásy, F. Galbrecht, A. Charas, J. Morgado, H. D. Burrows, U. Scherf, and A. P. Monkman, Macromolecules **39**, 6505 (2006).

[11] C. C. Kitts and D. A. Vanden Bout, Polymer **48**, 2322 (2007).

[12] M. Knaapila, F. B. Dias, V. M. Garamus, L. Almásy, M. Torkkeli, K. Leppänen, F. Galbrecht, E. Preis, H. D. Burrows, U. Scherf, and A. P. Monkman, Macromolecules **accepted** (2007).

[13] G. Fytas, H. G. Nothofer, U. Scherf, D. Vlassopoulos, and G. Meier, Macromolecules **35**, 481 (2002).

[14] M. Knaapila, R. Stepanyan, M. Torkkeli, B. P. Lyons, T. P. Ikonen, L. Almásy, J. P. Foreman, R. Serimaa, R. Güntner, U. Scherf, and A. P. Monkman, Phys. Rev. E **71**, 041802 (2005).

[15] E. Somma, B. Loppinet, C. Chi, G. Fytas, and G. Wegner, Phys. Chem. Chem. Phys. **8**, 2773 (2006).

[16] F. B. Dias, M. Knaapila, A. P. Monkman, and H. D. Burrows, Macromolecules **39**, 1598 (2006).

[17] L. Wu, T. Sato, H.-Z. Tang, and M. Fujiki, Macromolecules **37**, 6183 (2004).

[18] M. J. Banach, R. H. Friend, and H. Sirringhaus, Macromolecules **37**, 6079 (2004).

[19] M. Ballauff, Macromolecules **19**, 1366 (1986).

[20] M. H. Rahman, C.-Y. Chen, S.-C. Liao, H.-L. Chen, C.-S. Tsao, J.-H. Chen, J.-L. Liao, V. A. Ivanov, and S.-A. Chen, Macromolecules **40**, 6572 (2007).

[21] S. H. Chen, A. C. Su, C. H. Su, and S. A. Chen, Macromolecules **38**, 379 (2005).

[22] S. H. Chen, A. C. Su, and S. A. Chen, J. Phys. Chem. B **109**, 10067 (2005).

[23] W. Chunwaschirasiri, B. Tanto, D. L. Huber, and M. J. Winokur, Phys. Rev. Lett. **94**, 107402 (2005).

[24] M. Arif, C. Volz, and S. Guha, Phys. Rev. Lett. **96**, 025503 (2006).

[25] C. Rothe, S. M. King, F. Dias, and A. P. Monkman, Phys. Rev. B **70**, 195213 (2004).

[26] C. Rothe, F. Galbrecht, U. Scherf, and A. Monkman, Adv. Mater. **18**, 2137 (2006).

[27] A. Subbotin, M. Saariaho, O. Ikkala, and G. ten Brinke, Macromolecules **33**, 3447 (2000).

[28] R. Stepanyan, A. Subbotin, M. Knaapila, O. Ikkala, and G. ten Brinke, Macromolecules **36**, 3758 (2003).

[29] A. Subbotin, R. Stepanyan, M. Knaapila, O. Ikkala, and G. ten Brinke, Eur. Phys. J. E. **12**, 333 (2003).

[30] S. T. Milner, T. A. Witten, and M. E. Cates, Macromolecules **21**, 2610 (1988).

[31] H. Cheun, F. Galbrecht, B. S. Nehls, U. Scherf, and M. J. Winokur, J. Lumin. **122-123**, 212 (2007).

[32] H. B. Stuhrmann, N. Burkhardt, G. Dietrich, R. Junemann, W. Meerwinck, M. Schmitt, J. Wadzack, R. Willumeit, J. Zhao, and K. H. Nierhaus, Nucl. Instr. & Meth. A. **A356**, 124 (1995).

[33] G. D. Wignall and F. S. Bates, J. Appl. Cryst. **20**, 28 (1987).

[34] K. S. Vahvaselkä, R. Serimaa, and M. Torkkeli, J. Appl. Cryst. **28**, 189 (1995).

[35] O. Glatter, J. Appl. Cryst. **10**, 415 (1977).

[36] J. S. Pedersen, Adv. Colloid Interface Sci. **70**, 171 (1997).

[37] G. Porod, in *Small Angle X-ray Scattering*, edited by O. Glatter and O. Kratky (Academic Press, London, 1982).

[38] S. I. Hintschich, C. Rothe, S. Sinha, A. P. Monkman, P. Scandiucci de Freitas, and U. Scherf, J. Chem. Phys. **119**, 12017 (2003).

[39] H. Iloukhani and M. Rezaei-Sameti, J. Molec. Liq. **126**, 62 (2006).

[40] R. Boese, H.-C. Weiss, and D. Bläser, Angew. Chem. Int. Ed. **38**, 988 (1999).

[41] D. J. Abdallah and R. G. Weiss, Langmuir **16**, 352 (2000).

[42] M. Berghmans, S. Thijs, M. Cornette, H. Berghmans, F. C. De Schryver, P. Modenaers, and J. Mewis, Macromolecules **27**, 7669 (1994).